Available online at www.sciencedirect.com
SCIENCE DIRECT
International Journal of Machine Tools & Manufacture 45 (2005) 1577–1587
INTERNATIONAL JOURNAL OF MACHINE TOOLS & MANUFACTURE DESIGN, RESEARCH AND APPLICATION
www.elsevier.com/locate/ijmactool

Thermo-mechanical model with adaptive boundary conditions for friction stir welding of Al 6061

Vijay Soundararajan, Srdja Zekovic, Radovan Kovacevic*

Research Center for Advanced Manufacturing, Department of Mechanical Engineering, Southern Methodist University, 1500 International Parkway, Suite 100, Richardson, TX 75081 USA

Received 5 January 2005; accepted 15 February 2005
Available online 21 April 2005

Abstract

Thermo-mechanical simulation of friction stir welding can predict the transient temperature field, active stresses developed, forces in all the three dimensions and may be extended to determine the residual stress. The thermal stresses constitute a major portion of the total stress developed during the process. Boundary conditions in the thermal modeling of process play a vital role in the final temperature profile. The heating and cooling rates with the peak temperature attained by the workpiece determine the thermal stress. Also, predicting realistic peak temperature becomes important as the operating temperature at the interface of tool-workpiece is very close to the solidus temperature of the aluminum workpiece.

The convection heat-transfer coefficients of the surfaces exposed to air can be theoretically determined using Newton's law of cooling. Contact conductance depends on the pressure at the interface and has a non-uniform variation. The actual pressure distribution along the interface is dependent on the thermal stress from local temperature and non-linear stress–strain state. Therefore, applying an adaptive contact conductance can make the model more robust for process parameter variations.

A finite element thermo-mechanical model with mechanical tool loading was developed considering a uniform value for contact conductance and used for predicting the stress at the workpiece and backplate interface. This pressure distribution contours are used for defining the non-uniform adaptive contact conductance used in the thermal model for predicting the thermal history in the workpiece. The thermo-mechanical model was then used in predict stress development in friction stir welding.

Keywords: Friction stir welding; Heat transfer; Thermal modeling; Finite element analysis; Aluminum alloys; Contact conductance

1. Introduction

Friction Stir Welding (FSW) is a solid-state welding technology that has proven to be very effective for joining non-ferrous materials such as aluminum alloys, copper, and magnesium [1,2]. Recently, joining high melting point metal like steel using FSW has been reported [3]. The process is typically solid-state, meaning that the process operates below the solidus temperature of the metals being joined and no melting occurs during the process. FSW can produce welds that are high in quality, strong, and inexpensive to make with absence of oxidation and porosity. FSW delivers many advantages over conventional fusion welding processes such as no fumes, no welding arc, low heat input, and almost no weld finishing costs. FSW is being successfully applied to the aerospace, automobile, and shipbuilding industries [4].

Heat is generated at the contact between rotating tool and workpiece that plasticizes the material of workpiece under it. This softened material is subjected to extrusion by the tool pin rotational and transverse movements leading to formation of weld nugget. The temperature distribution in workpiece is very important as it affects the thermal stresses development in FSW process. The stress and strain field includes thermal stresses induced to the joint during the welding process and is responsible for the residual stress distribution, and the displacement field resulting in the final distortion of the weld joint.

In the last decade, a number of researchers [5–16] have been working on the modeling of heat transfer during FSW.

* Corresponding author. Tel.: +1 214 768 4873; fax: +1 214 768 0812.
E-mail address: kovacevi@seas.smu.edu (R. Kovacevic).

0890-6955/$ - see front matter © 2005 Elsevier Ltd. All rights reserved.
doi:10.1016/j.ijmachtools.2005.02.008

Nomenclature

c	heat capacity (J/kg K)
F_n	applied vertical force (N)
N	tool rotation (rpm)
μ	friction coefficient
R_s	radius of shoulder (m)
R_p	radius of pin (m)
H_p	height of pin (m)
ρ	density (kg/m^3)
T	temperature (K)
T_{amb}	ambient temperature (K)
δ	separation between plates (m)
v_x	velocity of moving heat flux (m/s)
k_T	thermal conductivity of the tool material (W/m K)
k_W	thermal conductivity of the workpiece material (W/m K)
k_x, k_y, k_z	thermal conductivity (W/m K)
q_1	heat generation at tool–shoulder interface(W)
q_2	heat generation at pin tip (W)
q_3	heat generation at the side of pin (W)
q_T	heat input into tool (W)
q_W	heat input into workpiece (W)
q_{int}	heat generation at contact between tool and workpiece (W)
q_{wb}	heat transfer between workpiece and backing plate (W)

Chao and Qi [5] presented a three-dimensional heat transfer model for the workpiece assuming a constant heat flux from the tool shoulder and a trial-and-error procedure to adjust the heat input until all the calculated temperatures matched with the measured ones. Frigaard et al. [6,7] developed a process model for the workpiece based on the finite difference method with a moving heat source. Bendzsak et al. [8,9] used the finite difference method in modeling the heat transfer and material flow process for a friction stir welded workpiece assuming the material to be a non-Newtonian fluid. Gould and Feng [10] used the Rosenthal equation for developing an analytical model for the heat transfer of the workpiece during FSW. Khandkar et al. [11] modeled the heat transfer to the workpiece for FSW lap welding with a moving heat source from the tool shoulder. Song and Kovacevic [12] presented a more detailed three-dimensional heat transfer model for both the tool and workpiece based on a finite difference scheme to simulate the transient temperatures. The heat input from the tool pin is modeled as a moving heat source [13,14], and the heat-transfer process of the tool and workpiece is indirectly coupled at the interface. Colegrave [16] uses an advanced analytical estimation of the heat generation for tools with a threaded tool pin to estimate the heat generation. Schmidt et al. [17] presented analytical equations for heat generation at the tool-workpiece interface and the heat generated by the pin taking sliding/sticking contact conditions into consideration.

Previous published thermal models consider the selection of backing plate to have a significant influence on the thermal history of the workpiece, as the backing plate with high thermal conductivity would allow more heat loss than the plate with low thermal conductivity. The workpiece-backing plate contact conductance is one the uncertain aspect of the thermal model as it cannot be determined accurately with experiments. The contact conductance value is assumed in the most of the previous thermal models as a fixed uniform value. Shi et al. [18] modeled the contact conductance as temperature dependent. The contact conductance value also depends on contact pressure in the workpiece-backplate interface and varies in non-uniform fashion as contours of decreasing value from the surface of workpiece right under the tool. As the tool moves, these non-uniform contours have to be redefined for the new tool position. Adaptable non-uniform contact conductance will result in better thermal model that can be used to predict the active stress development in the workpiece.

In the present work, a thermo-mechanical model is developed with both tool and workpiece using mechanical loading with thermal stress to predict the effective stress development at the bottom of workpiece with uniform boundary conditions. The stress is then used to define the adaptable contact conductance values in the thermal model at the workpiece-backing plate interface. The temperatures measured using thermocouples at various locations during experiment is used to validate the finite element model predictions.

2. Process details

Two 6061-T6 Al alloy plates, each with a dimension of $200\times50\times6.4$ mm^3 are butt welded in an adapted vertical milling machine for FSW. Fig. 1 shows the picture of the whole setup used for FSW. The tool made of CPM 1V tool steel, consists of a shank, shoulder, and pin with radii of 9.5, 12, and 2.6 mm, respectively. The three-dimensional view of the workpiece and tool with its boundary conditions is shown in Fig. 2. The temperature dependent material properties of aluminum alloy 6061-T6 [19,20] and CPM 1V tool steel [21] are considered during the model development and the plots as shown in Fig. 3.

During the FSW process, a rotating tool with pin is inserted in the material, and the tool traverses along the joint line. Friction between the rotating tool and workpiece during the rotary motion generates heat that creates a soft

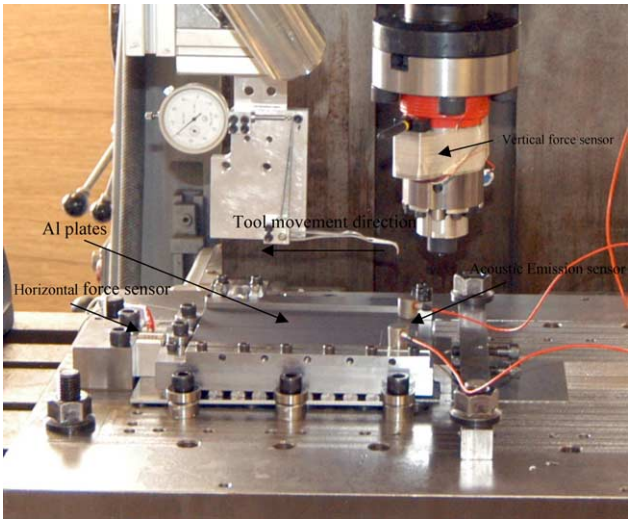

Fig. 1. Fixture for FSW with horizontal and vertical load measuring sensors.

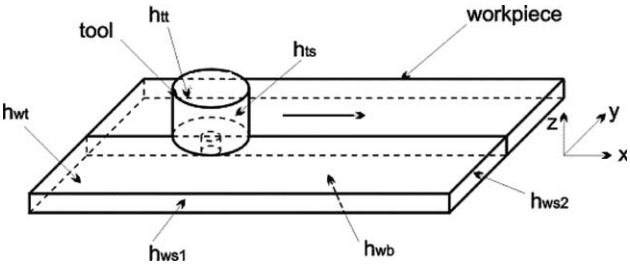

Fig. 2. Boundary conditions applied on tool and workpiece.

and plasticized region around the pin and tool shoulder. A weld is produced by extrusion of the plasticized material from the advancing side to the receding side of the weld. FSW experiments are performed varying the tool rotational speed and the traverse speed. The setup consists of a fixture to clamp the two plates together. One end of the fixture contains a horizontal load sensor, and the rotating tool holder has a vertical load cell with a load range of 0–44.5 kN. The forces measured from the experiment are used for the calculation of the heat input into the tool and workpiece.

3. Force and temperature measurements

Experiments are conducted under different welding parameters in order to use the measured temperature results for verification of the accuracy of the modeled ones. Four cases are considered with differing traverse speeds and tool rotations. A two-component dynamometer, based on strain gauge type force sensors is used for measuring the vertical and horizontal forces during the FSW process. The sensor for the vertical force measurement is fixed on the rotating tool, and a radio transmitter is used for transmitting the analog force data to the antenna receiver attached to the DAQ board. The control of the FSW operation is manual and may cause instability when maintaining a constant value of vertical force applied to the workpiece. Fig. 4 shows the vertical force measured from the FSW process for different rotational and traverse speeds. The sampling frequency of data for force measurement is 10 Hz.

The plates are prepared to measure the temperature at four points using thermocouples. On each plate, four 1.5 mm diameter holes were drilled on one side of the plate. Type K thermocouples of 1 mm diameter are subsequently inserted into the holes and glued so that the thermocouple ends are in intimate contact with the workpiece. The locations of thermocouples in the workpiece are shown in Fig. 5. Thermocouples connected to the channels 1–4 (Fig. 5) are used for the purpose of measuring the temperature at various positions on the workpiece. Two of these thermocouples (channels 1 and 2) are located in

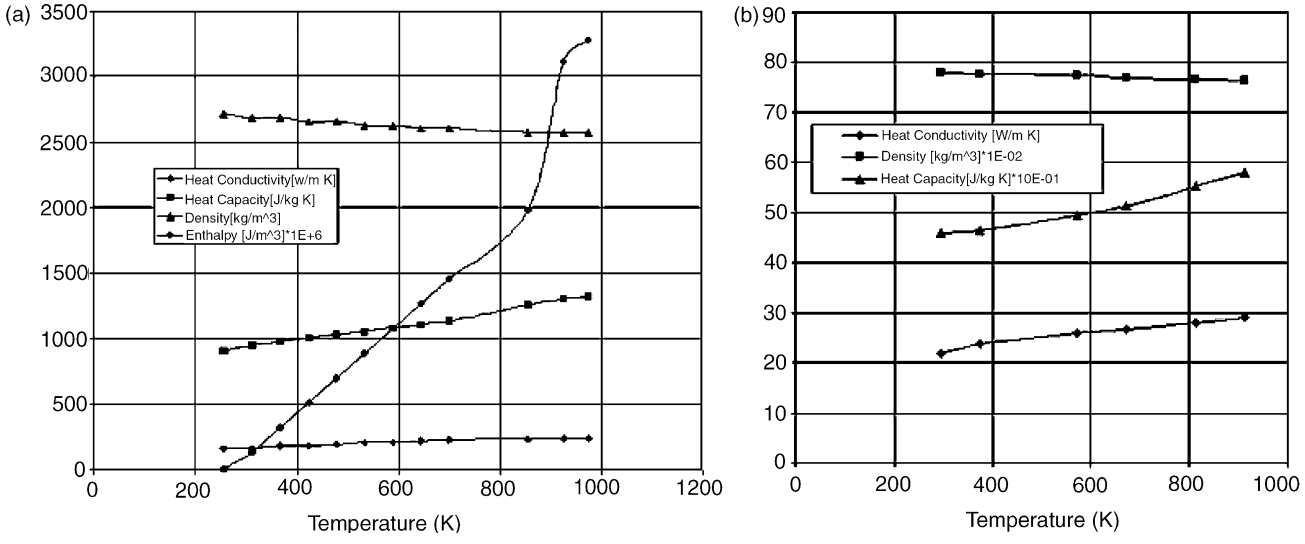

Fig. 3. Material properties of (a) Al 6061-T6 used in model [19,20] and (b) CPM 1V tool steel used in model [21].

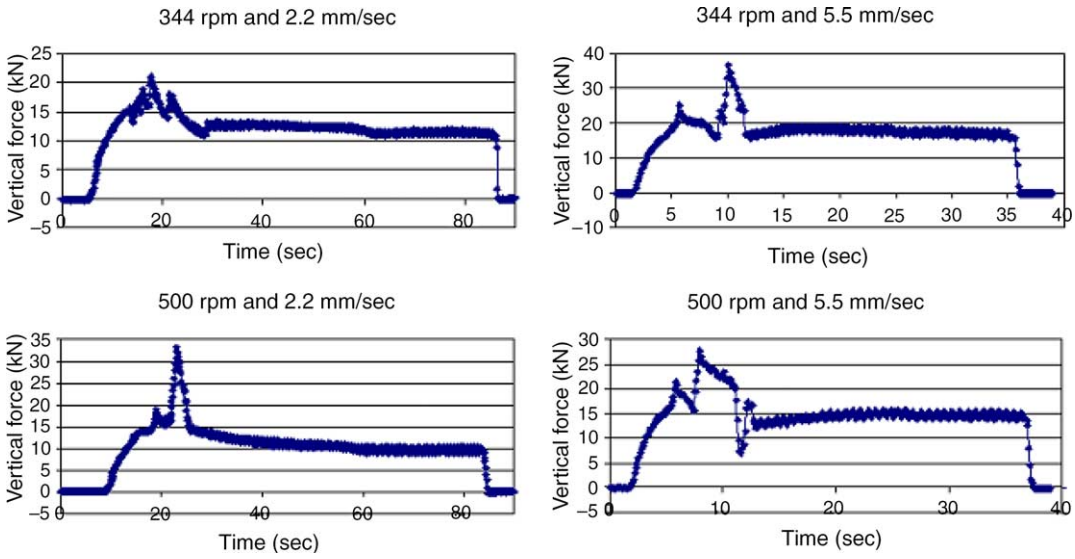

Fig. 4. Vertical force on the workpiece during FSW.

the heat-affected zone (HAZ), and the other two thermocouples (channels 3 and 4) are located in the base metal region. The thermocouples cannot be placed in the thermo-mechanically affected zone (TMAZ) of the weld, as the stirring action will displace it before it attains the maximum temperature in its location.

Transient temperatures are recorded in the four channels during the FSW process. Thermocouples are attached to a DAQ system that can sample the temperature data at 60 Hz. Data collection is accomplished with two DAQ systems, one for temperature and other for force, that are attached to a personal computer with a customized program running on LabView Software.

4. Model description

The FSW process is divided into the following three phases: (a) the penetration phase, (b) the welding phase and (c) the tool pull-out phase. The heat is generated due to friction and plastic deformation at the tool and workpiece interface during the process. During the welding period, the tool is moving at a constant speed along the joint line.

The assumptions made when defining the loads and boundary conditions for the simulation are (i) the coefficient of friction is assumed to vary between 0.4 and 0.5 based on the surface temperature at the contact of tool and workpiece; (ii) the tool pin is assumed to be cylindrical, and only its thermal effect is considered in the model; (iii) the radiation heat loss is neglected as it is considerably less compared to the conduction and convection losses.

The finite element thermo-mechanical model uses the temperature varying material properties (thermal conductivity, specific heat and density) for both the tool and workpiece. There is assumed to be no material melting since the maximum temperature is maintained below the solidus temperature (582 °C) of the aluminum alloy. Enthalpy values are not considered in the model.

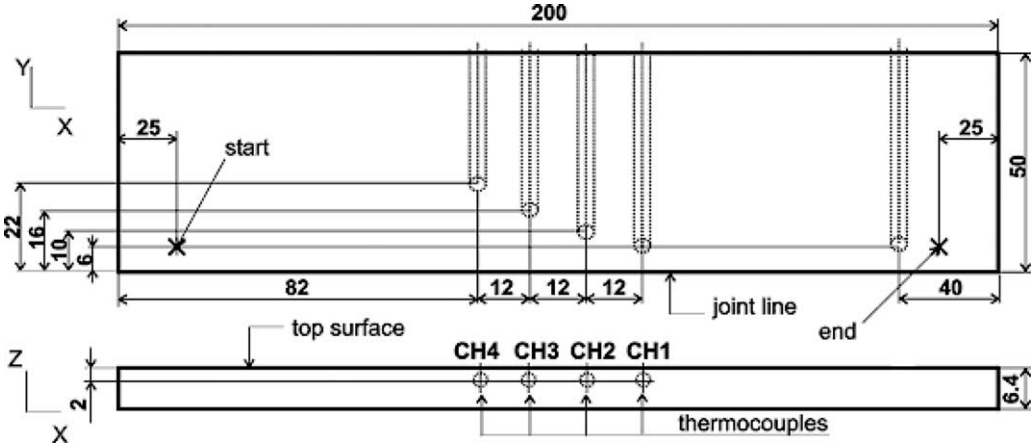

Fig. 5. Thermocouple positions on workpiece.

4.1. Heat transfer model

The main heat source in FSW is generally considered to be the friction between the rotating tool and the welded plates, and the 'cold work' in the plastic deformation of the material in the vicinity of the tool The heat generation from the plastic deformation of the material is considered to some extent in the model with the use of variable friction coefficient and not explicitly accounted for as a heat source.

The heat generated at the surface of the tool is transferred into the tool following the Fourier's law of heat conduction. The heat transfer equation for the tool in a static coordinate system is:

$$\rho c \frac{\partial(T)}{\partial t} = \frac{\partial}{\partial x}\left(k_x \frac{\partial T}{\partial x}\right) + \frac{\partial}{\partial y}\left(k_y \frac{\partial T}{\partial y}\right) + \frac{\partial}{\partial z}\left(k_z \frac{\partial T}{\partial z}\right) \quad (1)$$

where T is the temperature, c is heat capacity, ρ is the density and k_x, k_y, k_z are heat conductivities that vary with temperature in the calculations. The aluminum workpiece is considered to have isotropic material property and same value of thermal conductivity is used for all three directions.

The coordinate system moves over the workpiece in the positive x-axis at a velocity v_x. The heat transfer equation for the workpiece is:

$$\rho c\left(\frac{\partial T}{\partial t} + v_x \frac{\partial T}{\partial x}\right) = \frac{\partial}{\partial x}\left(k_x \frac{\partial T}{\partial x}\right) + \frac{\partial}{\partial y}\left(k_y \frac{\partial T}{\partial y}\right) + \frac{\partial}{\partial z}\left(k_z \frac{\partial T}{\partial z}\right) \quad (2)$$

where T is the temperature, c is heat capacity, ρ is the density, k_x, k_y, k_z are heat conductivities, and v_x is the welding speed.

The conduction and convection coefficients on various surfaces play an important role in the determination of the thermal history of the workpiece in friction stir welding. The initial and boundary conditions considered in our model are based on the actual conditions exhibited in experiments with the FSW setup shown in Fig. 1.

Fig. 2 shows the various boundary conditions applied on the model. Convection at the sides of the workpiece and tool is represented based on Newton's law of cooling as:

$$k \frac{\partial T}{\partial n}|_{\Gamma} = h(T - T_{\text{amb}}) \quad (3)$$

where n is the normal direction vector of boundary Γ and h is the convection coefficient. The convection coefficient is $h_{\text{ws 1}}$ at the sides of the workpiece parallel to the weld direction, $h_{\text{ws 2}}$ at the sides of workpiece perpendicular to the weld direction, h_{wt} at the top surface of workpiece exposed to ambient, h_{tt} at the sides of tool, at the top surface of tool connected to the shank.

Contact conductance at the interface of workpiece and backing plate has a non-uniform variation depending on the temperature and pressure at various zones in contact. The contact stress or pressure at interface varies laterally and longitudinally, as there is a moving vertical force transferred from the tool to the workpiece, a horizontal force due to the movement of the tool in positive x-axis and the clamps on two sides of the workpiece and also due to thermal stress development in the workpiece during the process. Superposition of mechanical loading on the workpiece with the thermal stress amplifies the vertical stress component during welding.

Contact conductance between the workpiece and backing plate is assumed to be a function of the contact stress between them.

$$h_{\text{tb}} = f(s_z) \quad (4)$$

where h_{tb} is the convection coefficient between the workpiece bottom and backing plate, and s_z is the contact stress in the z-axis.

The workpieces are clamped on its sides and only the tool exerts a pressure on the top surface. Due to lack of clamping forces on the top surface, there exists areas of positive stress and smaller negative stress exhibiting gap formation or great decrease in the contact pressure [22] at the interface of workpiece and backing plate. This leads to a large thermal resistance across the interface. Such a thermal resistance will dominate the heat transfer process when the contact bodies are good conductors and/or interstitial gaseous (or vacuum) medium has a very low thermal conductivity. A guideline for assuming the value of this gap is provided by Holman [23]. The equivalent convection coefficient for the workpiece/backing plate interface is calculated based on Eq. 5 [23]

$$q_{\text{wb}} = h_{\text{wb}}(T_1 - T_2) = Nu_{\delta}\frac{k}{\delta}(T_1 - T_2) \quad (5)$$

where Nu_{δ} is the Nusselt number (is equal to 1 when heat transfer is through conduction alone), k is the coefficient of conduction for the air/vacuum in the gap, δ is the separation distance between plates, T_1 is the average temperature of the workpiece, and T_2 is the temperature of the backing plate.

Frigaard et al. [24] states that during the welding period, heat generation equations can be directly used in the model development as long as the contribution from plastic deformation and the variable frictional conditions at the tool/workpiece interface are accounted for by the reasonable average value for friction coefficient. In the case of aluminum alloys, the local melting will occur if the material is heated above its solidus temperature. However, from the temperatures obtained in the workpiece from our experiments and from previous work, it is generally understood that the workpiece never reaches its solidus temperature. The friction coefficient is assumed to change between 0.4 and 0.5. Frigaard et al. [24] use the coefficient of friction value as 0.5 for the condition of sticky friction and 0.4 for the condition of partial sliding and sticky friction. The friction coefficient is considered to decrease from 0.5 to 0.4 as the temperature increases at the interface of tool and workpiece.

4.2. Thermo-mechanical model

The thermal model was sequentially coupled to the mechanical model. Workpiece was constrained in movement based on actual experimental setup. The mechanical loading of tool was considered retaining the load step size used in the thermal model. The temperature history of the workpieces was considered in each load step with the mechanical loading to calculate the active stress developed in the workpieces.

Initially, the thermo-mechanical model was used to predict the stress in vertical direction at the contact between workpiece and backing plate using a temperature varying uniform contact conductance based on published data [25]. This model was solved using finite element analysis and resulting stress in vertical plane on the workpiece bottom was used to define the non-uniform contact conductance.

5. Finite element model

The general purpose finite element code ANSYS is used for solving the energy equations and carrying out analysis. The Lagrangian finite element formulation with a non-uniform mesh is used for the model. The thermal model uses a SOLID70 element that has eight nodes with a single degree of freedom, or temperature, at each node for the workpiece and uses a SOLID5 element (a three-dimensional coupled field element) by activating only the thermal degree of freedom for the moving tool. These elements are applicable to a three-dimensional, transient thermal analysis. A higher density of mesh is provided at the surface along the joint line due to the maximum expected temperature gradient. The aspect ratio of the elements in the tool and the part of workpiece right below the tool is maintained closer to one. The density of mesh gradually decreases going laterally from the joint line. The heat generation is calculated at the interface and flows into tool and workpiece based on the ratio of their thermal conductivities. The thermal model was sequentially coupled to mechanical model by changing the element type of workpiece to SOLID45 having the same mesh and load step size. The mechanical loading was applied at the top of the tool. The load was transferred to the workpiece through the contact-target elements CONTA173 and TARGE170 provided at the tool workpiece interface.

6. Simulation results and discussion

6.1. Normal stress at the interface of workpiece and backing plate

The thermo-mechanical model was constructed and solved sequentially coupling the thermal and mechanical modules with identical mesh and load step size. The boundary conditions for the thermal model is shown in Fig. 2. In the mechanical model, the corresponding thermal history of the workpiece and tool is applied before the start of each load step and mechanical loading is coupled to determine the total stress. The workpiece is clamped on its sides and the bottom portion is constrained with a backing plate. The heat generated at the interface due to friction and plastic deformation of workpiece flows into the workpiece and tool. The heat in the workpiece is dissipated through the backing plate and also from the convection to surrounding air. The stress consists of thermal stress, and a combination and elastic and plastic stress created due to plastic deformation. Fig. 6 shows the stress distribution in the z-direction on the bottom surface of the workpiece when the tool is moving along the central line of the workpiece. As the tool moves, the stress distribution on the bottom surface of the workpiece moves with it.

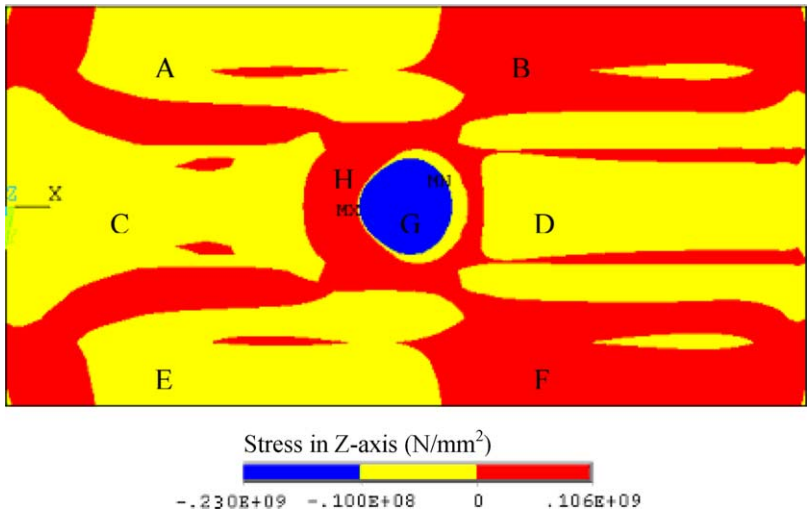

Fig. 6. Stress distribution at the bottom of workpiece.

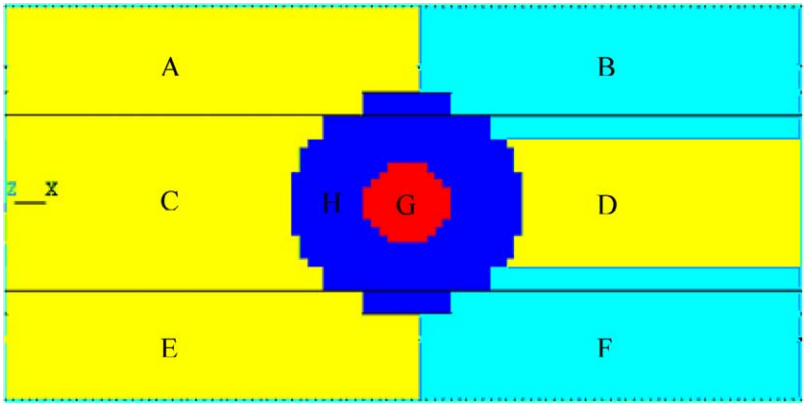

Fig. 7. Contours of convection coefficient applied at the bottom surface of workpiece.

6.2. Boundary conditions for thermal model

The top surface and the two sides of the workpiece that are lateral to the weld direction have free convection with ambient. The convection coefficients for these surfaces are calculated based on the theory of heat transfer for vertical plates [26] and horizontal plates [23,27]. Dickerson et al. [28] developed a thermal model for the tool and presented the values for the convection coefficient for the sides of the tool, and between the tool shank and tool holder. The calculated values of the convection coefficient for the tool based on Lienhard [29] are in good agreement with the convection coefficients used by Dickerson et al. [28]. This value of convection coefficients for tool was used in the thermal model.

6.3. Determination of non-uniform contact conductance

Contours of stress variation depends on the position of the tool. Fig. 6 shows the stress distribution at the bottom of workpiece. There are large islands of negative stress (pressure) right below the tool (region G), the surface behind and in front the tool (regions C and D), and the surface near the clamps in the area behind the tool. The negative stress zone right below the tool (region G) signifies a high compression between the workpiece and backing plate leading to a large contact conductance value in these surfaces. The remaining portions with positive stress zones in the area surrounding the tool (region H) and at the surface near clamps in front of the tool (regions B and F). These areas are created due to lack of clamping on the top surface of workpiece. There is a gap created due to thermal deformation of conforming surfaces of the workpiece and backing plate, and the contact conductance values are much smaller.

The value of the contact conductance is assumed to be in direct relationship with the stress distribution at the interface between the bottom surface of the workpiece and backing plate, and it moves with the tool. The gradient of the stress varies along the longitudinal and lateral directions in a non-linear fashion. It is difficult to apply contact conductance to exactly match the stress distribution variation. Based on the regions of varying contact conditions based on stress, a non-uniform contact conductance was modeled as shown in Fig. 7. The region with high compressive stress is region G below the tool. This region has the highest area contact conductance. The regions A, C, D and E have a much lower gradient of stress compared to region G. Based on the gradient of stress variation, an average value of the convection coefficient is

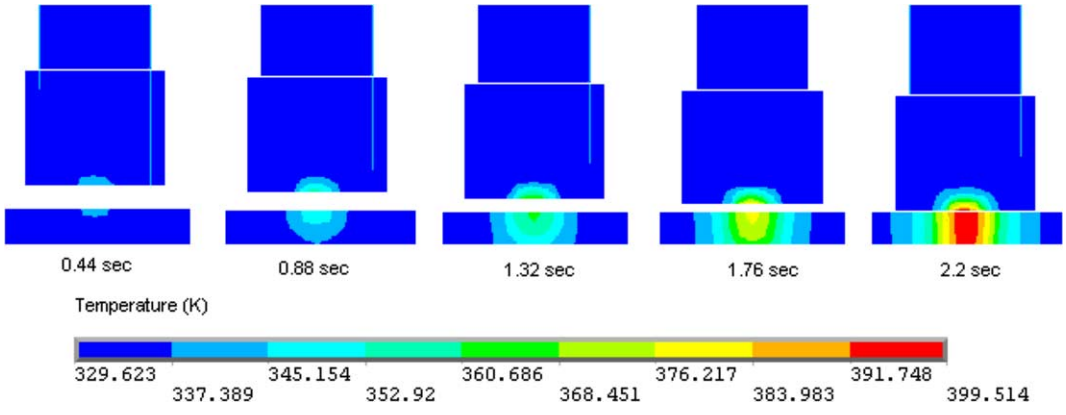

Fig. 8. Temperature–time history for tool and workpiece during tool pin penetration ($V=133$ mm/min, $\omega=344$ rpm).

Table 1
Input welding parameters for calculation

Coefficient of friction	Rotation speed (rpm)	Weld speed (mm/s)	Applied force (kN)
0.5	344	2.2	12.9
0.5	344	5.5	17.57
0.4	500	2.2	10.23
0.45	500	5.5	11.7

assumed using the plot from Rohsenow et al. [25] indicating the variation of the convection coefficient with the contact pressure for steel/aluminum. Assumed contact conductance below the tool was is in the range of 3000–4000 W/m^2 K. In the outer regions B and F in front of the tool shoulder, there exists a positive stress indicating the presence of a very small gap caused by warpage of the workpiece. Based on the assumption of gap, the contact conductance was calculated and assumed to be in the range of 30–300 W/m^2 K (Eq. (5)).

6.4. Thermal history

During the penetration phase, the rotating tool pin penetrates into the workpiece until the tool shoulder comes in contact with the workpiece. The penetration speed is chosen to be 2.22 mm/s in the model, and the corresponding penetration time is approximately 2.64 s. Fig. 8 presents cross-sectional views of the calculated temperature contours in the workpiece and tool at different times during the penetration. The cross-sectional views graphically illustrate the temperature history of the workpiece and the tool during the pin penetration.

The experiments are performed with different process parameters. The traverse speeds considered are 2.2 and 5.5 mm/s while the tool rotational speeds used are 344 and 500 rpm. Table 1 gives the input welding parameters used in the finite element calculation for four different initial conditions with their corresponding vertical force in the workpiece. The plasticization of material under the tool increases with increase in rotation speed and with decrease in tool traverse speed resulting the reduction of vertical force. The finite element simulation couples the moving tool with the workpiece and also considers the thermal effect of the initial tool pin penetration before the start of the weld. Simulations are performed initially with uniform contact conductance at the interface of workpiece and backing plate. Once the adaptive contact conductance profile was arrived at with its values, the simulations are performed again to determine the thermal history.

The longitudinal view of calculated temperature filed distribution along the joint line at the end of process is shown in Fig. 9. The results at the position of thermocouple in the simulated thermal profile at the end of the weld process is compared with the experimental results and shown in Fig. 10. It can be seen that the highest temperature attained is almost the same for both process simulations comparing well with the thermocouple results. But the gradient of temperature built-up in the workpiece is different for both the simulation cases, with adaptive contact conductance model giving closely conforming results.

6.5. Prediction of active stress

Stress is developed in the tool and workpiece during the process of welding because of thermal heating and cooling leading to thermal stress and application of mechanical loading with tool rotation and movement leading to structural stress generation. The thermo-mechanical model used for predicting the stress at the bottom of workpiece with uniform contact conductance, is now used with the adaptive contact conductance. The thermal results are input into the sequentially coupled mechanical model as body force. The tool movement on the workpiece was considered in the model with force applied on the top of the tool. Contact and target elements are used for maintaining the continuity in transfer of stress from tool to workpiece.

Fig. 11 shows the stress profile of the welded plate in three directions when tool reaches the middle of the workpiece. Fig. 11a shows active stress in longitudinal direction (X direction). It can be seen that the stress distribution in front of the plate (marked by A) is very less as it has not affected by thermal stress or by structural loading. In the area marked by C, it is observed that the tensile stress starts to increase due to the mechanical force in the horizontal direction and reaches maximum at the tool. The region behind the tool marked by D has a compressive stress with the maximum value right behind the tool. Due to the thermal expansion and constraint on the sides by the fixture results in compressive stress in this area. This stress extends till

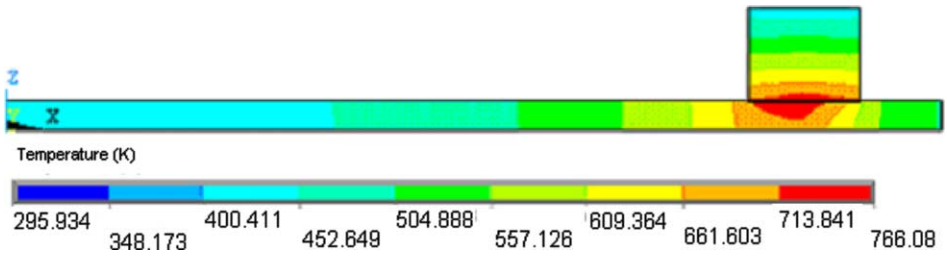

Fig. 9. Calculated temperature field distribution for the integrated tool-workpiece model in the longitudinal section along the joint line (V=133 mm/min, ω=344 rpm).

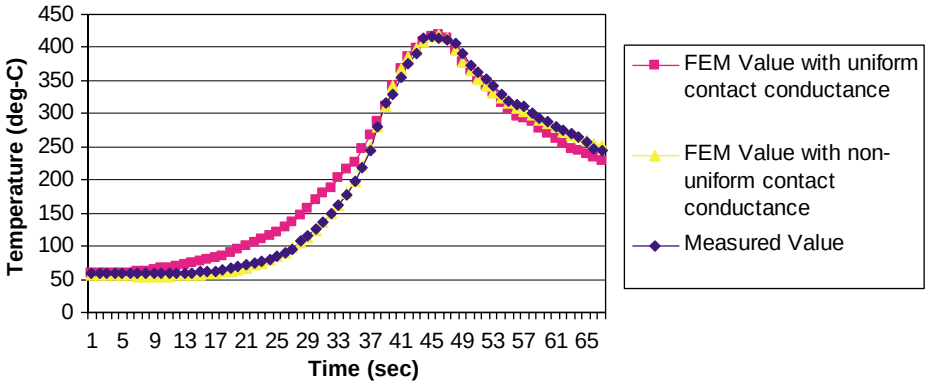

Fig. 10. Comparison of the modeled and the measured temperature history for workpiece. Temperature–time profile for thermocouple location 6 mm from the joint line ($V=133$ mm/min, $\omega=344$ rpm).

the region near the edge behind the tool. In the region marked by B, the compressive stress changes into tensile stress due to the shrinkage of workpiece, but clamped at the sides.

In Fig. 11b, the active stress in the transverse direction is shown (Y direction). There is very little tensile stress before the tool in the transverse direction as it is the stress development is due to tool movement along X axis which

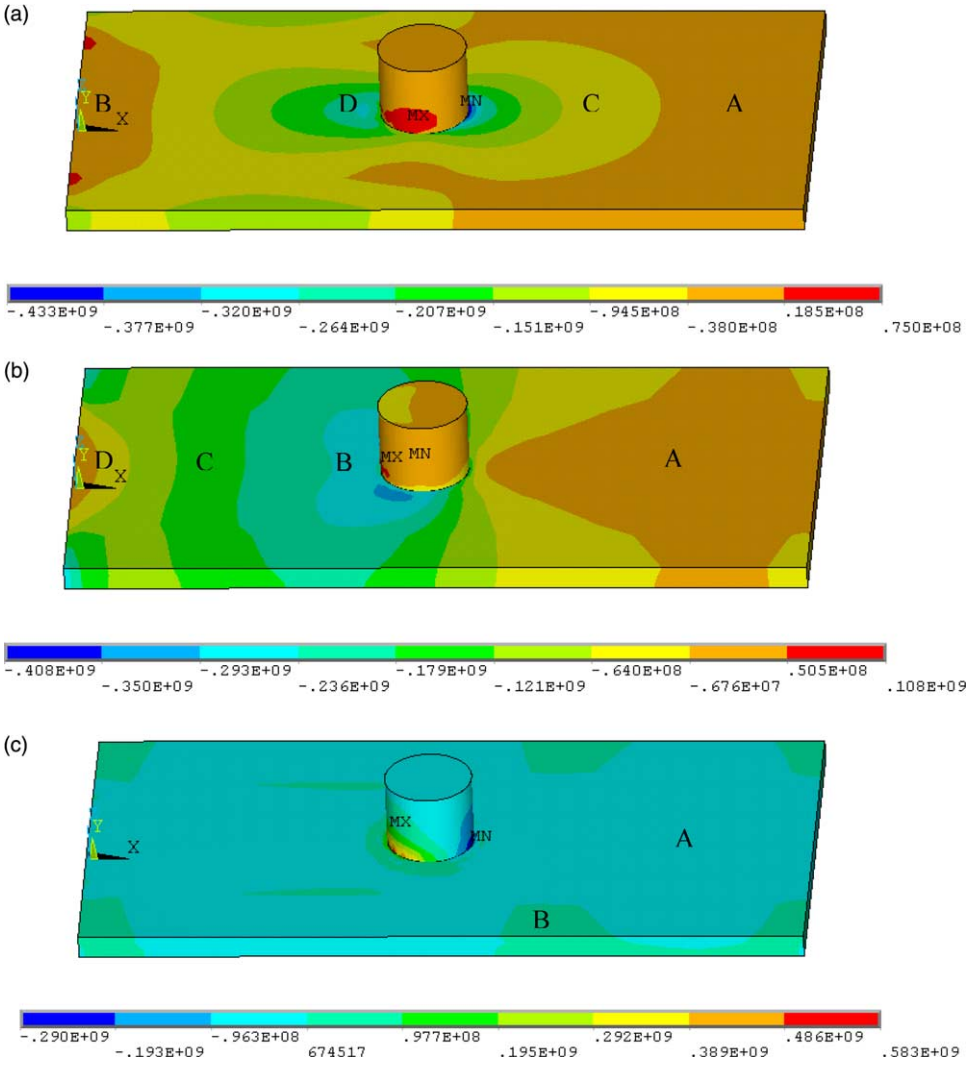

Fig. 11. Predicted stress distribution (N/mm^2) in the welded plate in three directions half way through the weld in (a) x axis (longitudinal direction) (b) y axis (lateral direction) (c) z axis (vertical direction).

mainly affects stress creation in longitudinal direction. The area behind the tool has a high compressive stress because of the thermal stress leading to expansion of workpiece which is constrained by fixture on both sides. It should also be noted that the transverse stress is spread over a very larger area behind the tool compared to that in longitudinal stress as the end of workpiece right behind the tool is not constrained leading to free thermal expansion. The region D has a tensile stress as the shrinkage of the workpiece has started to take place with constraints at the ends.

In Fig. 11c, it may be noted that the stress in the vertical direction is negligible along the edges of the workpiece (region B) while it is compressive in the remaining regions. There is a high compressive stress developed in the vertical direction on the tool as it moves forward. The region behind the tool exhibits a tensile stress because the surface of the tool is made have a complete contact with the workpiece. This tensile stress of higher order shown in simulation result may not be created in reality.

7. Conclusions

For determining the temperature at the interface of the tool shoulder and workpiece during the friction stir welding process, we have to relay on results of thermal simulation. The active stress in workpiece during the process leads to prediction of residual stress after the workpiece cools down and the clamps are removed. The dominant part of active stress is the thermal stress and its determination is based on the thermal model. The present paper develops a thermo-mechanical model to predict the thermal history and active stress with adaptive contact conductance at the interface of the workpiece and backing plate. The stress developed at the interface was determined considering uniform contact conductance and used to define the values and contours of the contact conductance. The contours were adaptively modified after each load step as the tool moves over the workpiece. Comparison of the temperature profile developed using adaptive and uniform contact conductance with the experimental results showed the possibility of more accurate determination using the present model. The workpiece surface temperature right under the tool reaches very close to the solidus temperature as seen from the obtained thermal results.

Acknowledgements

This work has been financially supported by General Motors Corporation and SMU's Research Center for Advanced Manufacturing, Richardson, TX. The authors would like to acknowledge Mr Michael Valant's contributions in carrying out the experiments for this research. The authors would like to thank Mr Steve Groothuis, Micron Technologies, Dallas, TX for his guidance during the model development.

References

[1] C.J. Dawes, W.M. Thomas, Friction stir welding for aluminum alloys, Weld. J. 75 (3) (1996) 41–45.
[2] E.D. Nicholas, S.W. Kallee, Causing a stir in the future, Welding and Joining, Feb 1998, pp. 18–21.
[3] T.J. Lienert, Friction stir welding of DH-36 steel, Proceedings from Materials Solutions 2003 on Joining of Advanced and Specialty Materials 2004; 28–34.
[4] E.D. Nicholas, Friction stir welding-a decade on, in: IIW Asian Pacific International Congress, Sydney, Australia, 29 Oct–2 Nov, 2000.
[5] Y. Chao, X. Qi, Thermal and thermo-mechanical modeling of friction stir welding of aluminum alloy 6061-T6, J. Mater. Proc. Mfg. Sci. 7 (1998) 215–233.
[6] O. Frigaard, O. Grong, Modeling of the heat flow phenomena in friction stir welding of aluminum alloys, in: Proceedings of the Seventh International Conference on Joints in Aluminum (INALCO '98), Cambridge, 15–17. April, 1998.
[7] O. Frigaard, O. Grong, A process model for friction stir welding of age hardening aluminum alloys, Metall. Mater. Trans. 2001; 32A.
[8] G.B. Bendzsak, T.B. North, C.B. Smith, An experimentally validated 3D model for friction stir welding, in: Proceedings of the Second International Symposium on Friction Stir Welding, Sweden, 2000.
[9] C.B. Smith, G.B. Bendzsak, T.H. North, J.F. Hinrichs, J.S. Noruk, R.J. Heideman, Heat and material flow modeling of the friction stir welding process in: T. Siewert, C. Pollock (Eds.), Proceedings of the Ninth International Conference on Computer Technology in Welding, Detroit, Michigan, May (2000), pp. 475–486.
[10] J.E. Gould, Z. Feng, Heat flow model for friction stir welding of aluminum alloys, Mater. Process. Mfg Sci. 7 (1998) 185–194.
[11] H. Khandkar, M. Zahedul, J. Khan, Thermal modeling of overlap friction stir welding for Al-alloys, J. Mater. Process. Mfg Sci. 10 (2) (2001) 91–106.
[12] M. Song, R. Kovacevic, Heat Transfer modeling for both workpiece and tool in the friction stir welding process: a coupled model, Proc. Instn Mech. Engrs. Part B: J. Eng. Manufacture 218 (2004) 17–33.
[13] M. Song, R. Kovacevic, Numerical and experimental study of the heat transfer process in friction stir welding, Proc. Instn Mech. Engrs. Part B: J. Eng. Manufacture 217 (81) (2003) 73–85.
[14] M. Song, R. Kovacevic, Thermal modeling of friction stir welding in a moving coordinate and its validation, Int. J. Machine Tool Manufacturing 43 (6) (2003) 605–615.
[15] C.M. Chen, R. Kovacevic, Finite element modeling of friction stir welding - thermal and thermomechanical analysis, Int. J. Machine Tools Manufacture 43 (2003) 1319–1326.
[16] P. Colegrove, Three-dimensional flow and thermal model-ing of the friction stir welding process, in: Proceedings of the Second International Symposium on Friction Stir Welding, Sweden, 2000.
[17] H. Schmidt, J. Hattel, J. Wert, An analytical model for the heat generation in friction stir welding, Model. Simul. Mater. Sci. Eng. 12 (2004) 143–157.
[18] Q. Shi, T. Dickerson, H.R. Shercliff, Thermo-mechanical FE modelling of friction stir welding of AL-2024 including tool loads, in: Proceedings of the Fourth International Symposium on Friction Stir Welding, Park city, UT, 2003.
[19] M. Song, Numerical simulation of heat transfer in friction stir welding, PhD Thesis, Southern Methodist University, 2003.
[20] http://www.matweb.com
[21] http://www.crucibleservice.com

[22] S.L. Lee, R. Ou, Gap formation and interfacial heat transfer between thermoelastic bodies in imperfect contact, J. Heat Transfer 123 (2001) 205–212.
[23] J.P. Holman, Heat Transfer, eighth ed. 1997. pp. 333–352 and 360–362.
[24] O. Frigaard, O. Grong, T. Midling, A process model for friction stir welding of age hardening aluminum alloys, Metall. Mater. Trans. A 32A (2001) 1189–1200.
[25] W.M. Rohsenow, J.P. Hartnett, E.N. Ganic, Handbook of Heat Transfer Fundamentals, second ed. 1985. pp. 4–19.
[26] F.P. Incropera, D.P. De Witt, Fundamentals of Heat and Mass Transfer, third ed., Wiley, New York, 1990. p. 543, Eqs. 9.26 and 9.27.
[27] T. Fujii, H. Imura, Natural convection heat transfer from a plate with arbitrary inclination, Int. J. Heat Mass Transfer 15 (1972) 755.
[28] T. Dickerson, Q. Shi, H.R. Shercliff, Heat flow into friction stir welding tools, Fourth International Symposium on Friction Stir Welding, Park city, UT, 14–16 May, 2003.
[29] J.H. Lienhard, A Heat Transfer Textbook, third ed., Phlogiston Press, 2003. pp. 418–419.